Nano Energy 63 (2019) 103852

Contents lists available at ScienceDirect

Nano Energy

journal homepage: www.elsevier.com/locate/nanoen

Full paper

Understanding the dynamic response in ferroelectret nanogenerators to enable self-powered tactile systems and human-controlled micro-robots

Yunqi Cao[a], José Figueroa[a], Wei Li[b], Zhiqiang Chen[c], Zhong Lin Wang[d], Nelson Sepúlveda[a,*]

[a] Department of Electrical and Computer Engineering, Michigan State University, East Lansing, MI, 48824, United States
[b] Department of Electrical Engineering and Computer Sciences, University of California, Berkely, Berkeley, CA, 94720, United States
[c] School of Mechano-Electronic Engineering, Xidian University, Xi'an, Shaanxi, 710071, China
[d] School of Materials Science & Engineering Georgia Institute of Technology, Atlanta, GA, 30332, United States

ARTICLE INFO

Keywords:
Ferroelectret
Nanogenerator
Impedance match
Dynamic response
Sensor array
Human control

ABSTRACT

Self-powered pressure sensors are critical devices in IoT sensing networks. Continuous efforts have been made in the community to improve the device performances by optimizing the materials selection and structural configurations. Therefore, a design platform for understanding the device-machine interface is imperative. This work presents a comprehensive study that uses the fundamental working principles of dipole moments in ferroelectret polymers to describe the energy conversion mechanism. The study addresses discrepancies in voltage measurements caused by instruments with different internal resistances and sampling rates. A lumped parameter model is also proposed and validated to explain the impedance mismatch at the device-machine interface. Applications including control of MEMS microactuator through static response and dynamic pressure sensor array for impact distribution sensing have also been demonstrated.

1. Introduction

Flexible pressure sensor arrays have demonstrated to have promising applications in sensing networks where the complex environmental stimulus is considered. Bio-compatible soft electronic skins that are capable of pressure distribution visualization have been exploited extensively in the field of soft robotics [1] and human motion monitoring [2–5]. Despite the different approaches in integrating each individual pixel sensing element, the functionality of each sensing unit can be classified into several groups according to its working principle. Generally, resistive, capacitive and piezoelectric mechanisms are often considered for various applications [6]. Resistive pressure sensors are most widely used in real applications due to their simple device structures, high S/N ratio, and easy readout features [7]. But the high sensitivity is usually limited to low pressure ranges (< 5 kPa) [8] and requires high power consumption. Capacitive pressure sensors measure different pressures by monitoring the capacitance variations, caused by the change in separation between parallel plates. By optimizing microstructures within each sensing element and the material's dielectric constant [9], capacitive sensors with high spatial resolution and large dynamic range have been developed [10,11]. However, the rather complicated evaluation system and the inherent hysteresis error still remain a problem. Pressure sensors based on piezoelectric effect convert a mechanical input to an electrical output upon change of the dipole moments. The high sensitivity can be achieved by improving the d_{33} coefficient. The compatibility with micro-fabrication techniques also makes it more adaptable to the high spatial resolution requirements [12,13]. Nevertheless, the large internal impedance restricts the applications in static pressure sensing [11,14].

Although the choice of pressure sensing technology is determined by specific applications, battery-based resistive and capacitive pressure sensors are not considered to be the optimal approaches for Internet of Things (IoT) devices, which impose the sensor network with lightweight, miniature size, and energy sustainability requirements. Therefore, a direct energy conversion between mechanical input and electrical sensing output becomes imperative. Nanogenerator-based self-powered pressure sensors using piezoelectric or triboelectric effect have been demonstrated as emerging technologies in flexible electronics [15,16]. Inorganic piezoelectric nanostructures are introduced by micro-fabrication techniques to improve the detecting sensitivity and sensing resolution. Nanowires (NWs) such as ZnO [17], CdS [18], and $NaNbO_3$ [19] with high electric output are often used as piezoelectric sensors. Mechanical energy from the bending motion of nanowires is converted to an electric output. Composite nanoparticles (NPs), e.g. $BaTiO_3$ [20,21], are also often used to improve the piezoelectric effect by increasing the total dipole moments. To overcome the low flexibility

* Corresponding author.
E-mail address: nelsons@egr.msu.edu (N. Sepúlveda).

https://doi.org/10.1016/j.nanoen.2019.06.048
Received 28 May 2019; Received in revised form 21 June 2019; Accepted 23 June 2019
Available online 27 June 2019

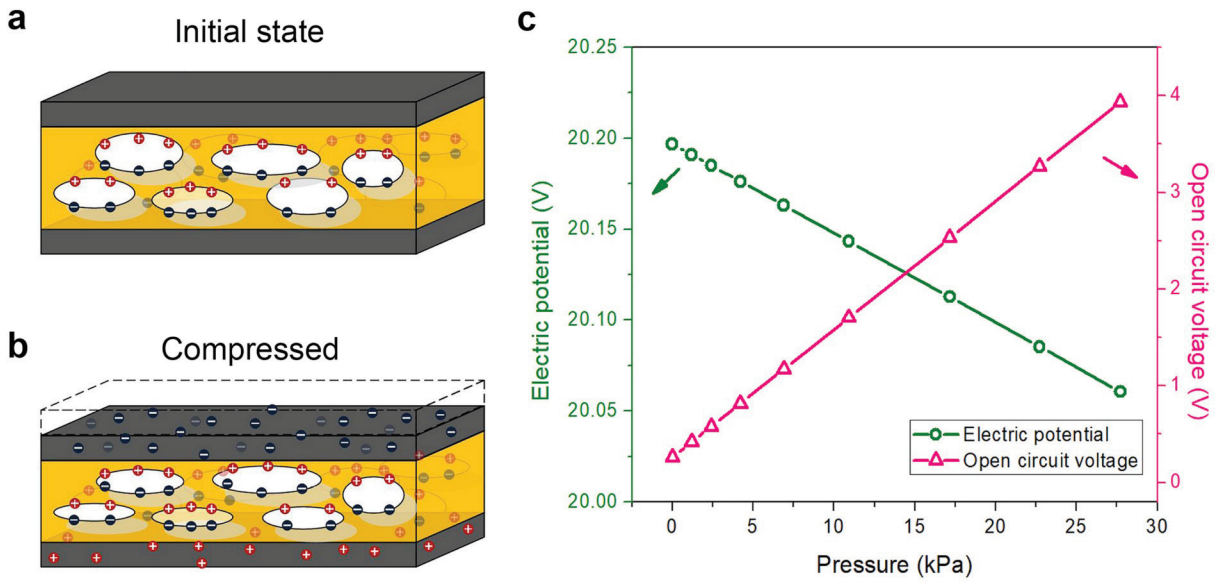

Fig. 1. Working principle of ferroelectric nanogenerator. (a) No external stress is applied. (b) When external boundary load is applied, the polarization field due to internal dipoles decreases and free induction charges are accumulated on metal electrodes. (c) FEM results of changes in electrode potential at the polymer-metal boundary and open circuit voltage arises from accumulated charges.

of inorganic piezoelectric nanogenerator (PENG) sensors, foldable and stretchable substrates such as polydimethylsiloxane (PDMS), polyethylene terephthalate (PET), or polyethylene (PEN) can be used [22]. Triboelectric sensors convert the mechanical energy by utilizing the internal friction of the material, the selection of the active materials are therefore broadened from NWs/NPs to polymers [23] and soft fabrics [24], which significantly improve flexibility. Their high performance has also been demonstrated by optimization of the microstructure such as surface etching [13], topology casting [25], injection molding, etc. However, most of the current researches are focused on improving the device's internal structures or materials [26], and little attention has been paid to the device-to-instrument interface, where the impedance match could significantly affect the energy conversion process. The cross-talk issue could still be a limiting factor for sensor array applications since most of the time a complicated patterning of each sensing element is required, and the triboelectric effect would also response to random mechanical inputs.

In this work, a self-powered piezoelectric pressure sensor based on polypropylene (PP) ferroelectret nanogenerator (FENG) [27–29] is presented. The high d_{33} (~ 300 pC/N) [30] value comes from the pre-charged micro-voids that are engineered inside the PP film. The energy conversion process from mechanical to electrical domain in terms of open circuit voltage (V_{oc}) and short circuit current (I_{sc}) are discussed in the point view of changing dipole moments which is analog to the piezoelectric effect. Single sensing element of 15 mm × 15 mm thin patch FENG device is characterized under different mechanical impacts provided by the vibration exciter. Various resistive loads are connected to the device for evaluating the performances under different impedance matches, which explain the different observations caused by instruments. A lumped electromechanical model and its equivalent circuit model are proposed to give a straightforward perspective of the dynamic response in the electrical domain. A prove-of-principle FENG based 4 × 4 sensor array is also presented to demonstrate the dynamic pressure mapping, each sensing pixel is defined by simply pattern the metal electrode with a shadow mask and no cross-talk issue is observed. Because of the different transduction behaviors under different impedance matches, a human controlled micro-robotic arm interface is also demonstrated based on the static pressure response. This work has potential contributions in understanding the platform of design device-machine interface and perspective measurement results from different instruments.

2. Results and discussion

FENG is a flexible multilayer structure device with the ability of converting mechanical energy to or from electrical energy. The active material that exhibits the direct and inverse piezoelectric effect is a dielectric and elastic film with full-of-cell type structure (See fabrication process in Fig. S1, Supporting Information). Despite that the FENG has a similar electrical-mechanical response as the piezoelectric nanogenerator, the fundamental working principles are different. By applying external mechanical pressure (F/A), the thickness of the porous midsection region of the polypropylene ferroelectret (PPFE) film decreases. The piezoelectricity of FENG mainly arises from the relative movement of positive charge surface to negative charge surface within each individual ellipsoid void. Each ellipsoid has a permanent dipole moment p_i which can be expressed as $p_i = q_i l_i$, where q_i is the trapped charges and l_i is the initial separation. For a FENG device of volume V and consisting of N ellipsoids, the initial permanent polarization field is therefore determined to be $P_0 = \Sigma_{i=1}^{N} p_i / V$. When external mechanical load is applied, the structure distortion causes a change in the void separation from l_i to l_i' and the polarization field needs to be modified as $P' = \Sigma_{i=1}^{N} p'_i / V = \Sigma_{i=1}^{N} q_i l_i' / V$. Thus, the change in the polarization field induces free charges on metal electrodes and can be expressed as: $Q = \Sigma_{i=1}^{N} q_i (l_i - l_i')/h$, where h is the thickness of the FENG. This expression for Q can be further rewritten as $Q = (F/EV)\Sigma_{i=1}^{N} p_i$, where F, E, and A are the applied force, Young's modulus of PPFE, and area, respectively. Since the FENG device shares a capacitive model [31,32], V_{oc} under F can be described as:

$$V_{oc} = \frac{hP_0}{\varepsilon EA} F, \tag{1}$$

where ε is the relative dielectric constant of PPFE. It can be seen from Eq. (1) that there is a linear coupling between V_{oc} and P (or F). As shown in Fig. 1a and b, the decrease in distance between the charged surfaces, from l_i to l_i', produces a relative movement of charges with different types. This change in dipole moments generates a displacement current and is accounted for the I_{sc} output under a short circuit condition,

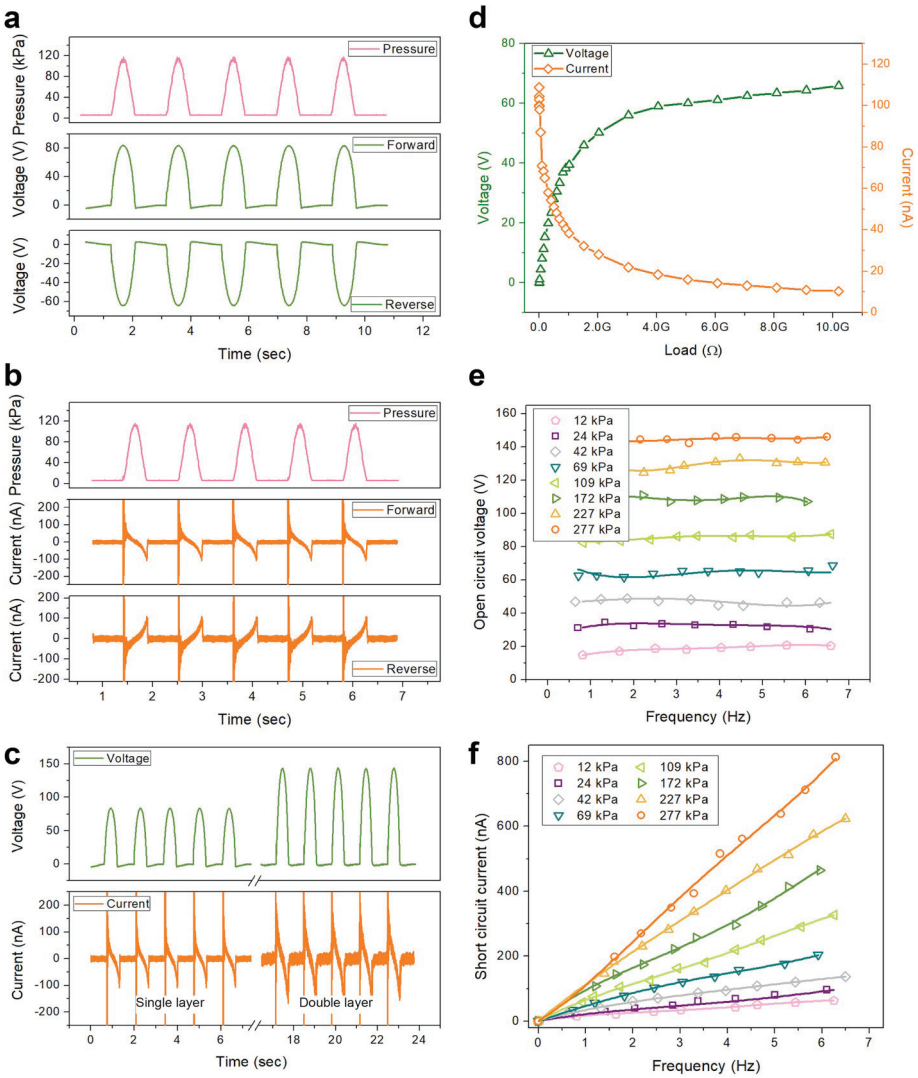

Fig. 2. Electromechanical characterization of FENG under sinusoidal pressure input. (a) Forward and reverse V_{oc} of FENG under sinusoidal pressure input. (b) Forward and reverse I_{sc} of FENG under sinusoidal pressure input. (c) Amplification of V_{oc} and I_{sc} of FENG by a symmetric folding process under sinusoidal pressure input. (d) Electric output, voltage and current, under sinusoidal pressure input with increasing resistive load. (e) V_{oc} of FENG under sinusoidal pressure input with variable pressure amplitudes and frequencies. (f) I_{sc} of FENG under sinusoidal pressure input with various pressure amplitudes and frequencies.

which can be expressed as:

$$I_{sc} = \frac{P_0}{E}\frac{\partial F}{\partial t}. \quad (2)$$

The derived expressions for V_{oc} and I_{sc} of FENG (Eqs. (1) and (2)) indicate that the open circuit voltage and short circuit current produced by FENG increase with compression load and rate of change in dipole moments, respectively. From this derivation, it follows that the electric output is frequency-dependent; but only in the I_{sc} term –not V_{oc}. This is explained and demonstrated experimentally in the next section. Some of the previously reported observations on frequency-dependent V_{oc} could be due to the use of low-input impedance instruments. Fig. 1c shows the electromechanical behavior of the PPFE film based on a 250 μm × 90 μm 2-D finite element method (FEM) model. At the initial state, the permanent polarization field induced boundary charges lead to an electric potential at the polymer-metal interface. When the compression load occurs, the polarization field is reduced due to the decrease in dipole moments. This results in a lower electric potential and therefore free charges accumulate on metal electrodes. Because the device shares a capacitive electrical model, the accumulated charges give rise to an open circuit voltage, which is dependent on the mechanical input.

The experimental demonstration of the parameters that determine the V_{oc} and I_{sc} of FENG follows. The electric outputs of FENG in terms of: *(i)* V_{oc}, *(ii)* I_{sc}, and *(iii)* voltage with resistive load (V_{load}) are measured during repetitive external mechanical inputs, which consists of both: pressing and releasing stages in each pulse. Since the open circuit voltage and short circuit current outputs will be different from those with a load, the input impedance of the equipment used to measure these two parameters (V_{oc} and I_{sc}) has an influence on the measurements (Fig. S5, Supporting Information). When measuring I_{sc}, an ammeter usually directly converts the input current to a reading through a galvanometer. Therefore the measurement is less dependent on the instrument's internal circuit and should be an accurate reading of the current when a short circuit is connected to the FENG. However, a voltmeter consists of a galvanometer with a large internal resistor connected in series. The obtained voltage reading is the input current flowing through the galvanometer times the internal resistance. Therefore using voltmeters with different internal resistances will result in different measurements (See Supporting Information for details). Specifically, using a voltmeter with lower internal resistance will show V_{oc} with two peaks during a single mechanical pulse input (one peak with positive magnitude in the pressing stage and one peak with negative magnitude in the releasing stage). According to Eq. (1), these two

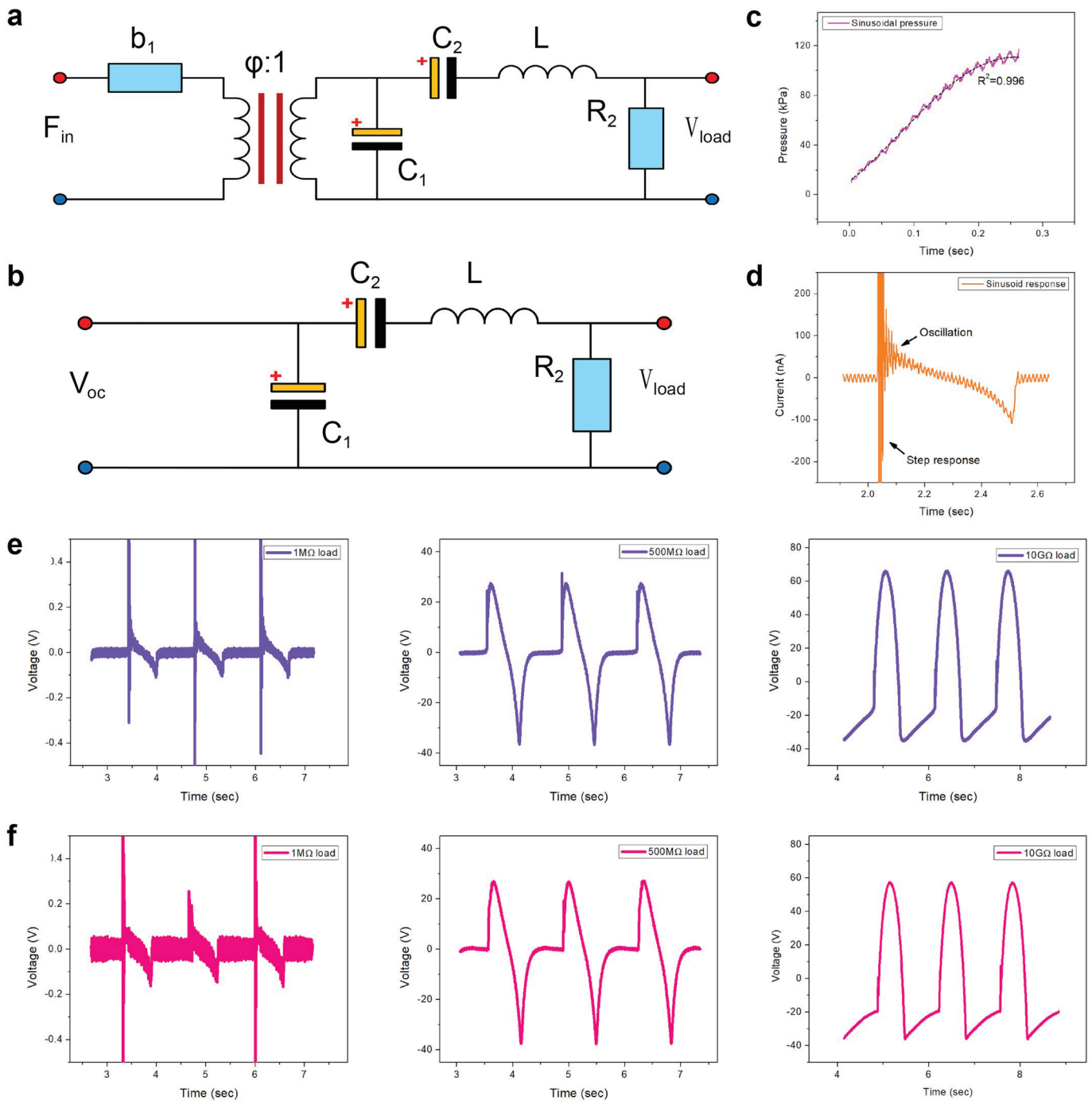

Fig. 3. Illustration of the lumped model. (a) Lumped electromechanical model of FENG. (b) Equivalent electrical circuit model of FENG. (c) Impact profile of a sinusoidal pressure input. (d) I_{sc} under a sinusoidal pressure input. (e) Experimental electromechanical response with different load resistances. (f) Simulated electromechanical response with different load resistances.

peaks of opposite signs do not correctly represent the physics of the process, since the releasing step also represents a pressure of positive magnitude - which should produce a positive V_{oc} output. In other words, the instant of peak pressure (i.e. the instant where pressing stops and releasing begins) should also represent a peak in the V_{oc} output (not $V_{oc} = 0\,V$). Considering the high impedance of the PPFE film in low frequency range, a testing instrument with much higher internal impedance is required for getting an accurate V_{oc} measurement. In this experiment, V_{oc} is measured by Keithley 2450 Source Measure Unit. The internal impedance of the voltmeter is in the trillion Ohm (TΩ) range which provides more accurate results.

The electric outputs under periodic nonlinear pressure inputs generated by a vibration exciter (Fig. S3, Supporting Information) are shown in Fig. 2. The changing polarity test is also carried out to confirm that the electric signal comes from the FENG. As shown in Fig. 2a and b, the electromechanical response of FENG exhibits a similar behavior as the piezoelectric effect. The V_{oc} follows the change of the external mechanical input while the I_{sc} is proportional to the derivative of the input according to Eqs. (1) and (2). An oscillation of exponentially decaying amplitude is observed at the rising edge of the signal (See Fig. 2b, c, Fig.3d, and Fig. S4 in Supporting Information). And the nearly infinite peak at the rising edge is related to the derivative of the sinusoidal

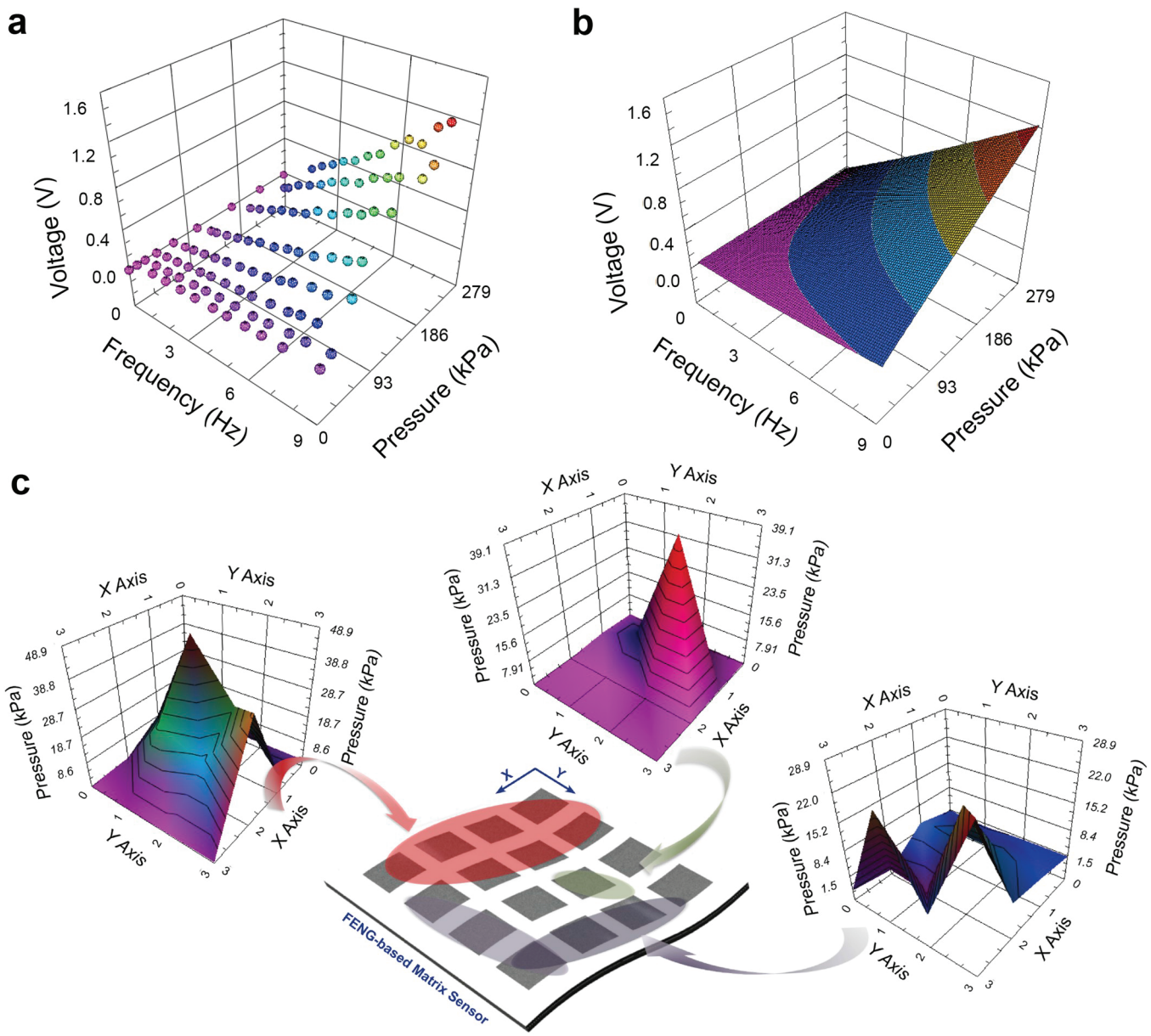

Fig. 4. FENG-based matrix pressure sensor. (a) Voltage output of a 15 mm × 15 mm single layer FENG as a function of input pressure amplitudes and frequencies. (b) 3D surface fitting of the single pixel electromechanical response, $R^2 = 0.93$. (c) 16-pixel FENG based matrix sensor and 3D contour maps of the pressure distribution over the sensor upon an impact from the user.

pressure input at $P = 0\ N$. The observed oscillation can be related to the mechanical properties of the PPFE film and the electrical impedance match which reveals the electromechanical model of the FENG. Also, it can be seen from Fig. 2c that folding a 30 mm × 15 mm patch of FENG along a symmetry axis into a smaller patch of 15 mm × 15 mm can double both the V_{oc} and I_{sc} for a given mechanical input.

The electric outputs under different resistive loads are also investigated and results are shown in Fig. 2d. A mechanical input with a pressure amplitude of 110 kPa and frequency of 1.7 Hz shows a voltage output that increases with resistive load, approaching V_{oc}. Fig. 2e and f show V_{oc} and I_{sc} as a function of pressure amplitude and frequency. V_{oc} increases with pressure amplitude but remains constant for different frequencies from a given pressure amplitude as indicated by Eq. (1). I_{sc}, on the other hand, increases with the changing rate of the mechanical input, which is related to pressure amplitude and frequency, as shown in Fig. 2f. These experimental results are consistent with the theoretical and conceptual rationale explained above.

Many lumped parameter models have been developed for different types of piezoelectric film materials in different operating frequency regions. In the low-frequency region, a simple RC model can be effectively used for modeling the electrical behavior [33]. For piezoelectric polymer, the internal resistance is nearly infinite, thus the electrical model is purely capacitive. Multiple electromechanical lumped models for piezoelectrics have been proposed, which consider the underlying physics and specific applications [34–36]. However, a lumped model for describing the electromechanical response of nanogenerators is still needed to analyze the electric output under different impact pressure profiles and resistive loads. The overshoot presented in the I_{sc} at the rising edge of the pressure input shown in Fig. 2b suggests a second order system model (Instrument with lower sampling rate may not capture this phenomenon, see Supporting Information for details). When an external mechanical stress is applied, a change in dipole moments of the mid-section layer is induced in terms of the charge separation. This produces a displacement current that is proportional to

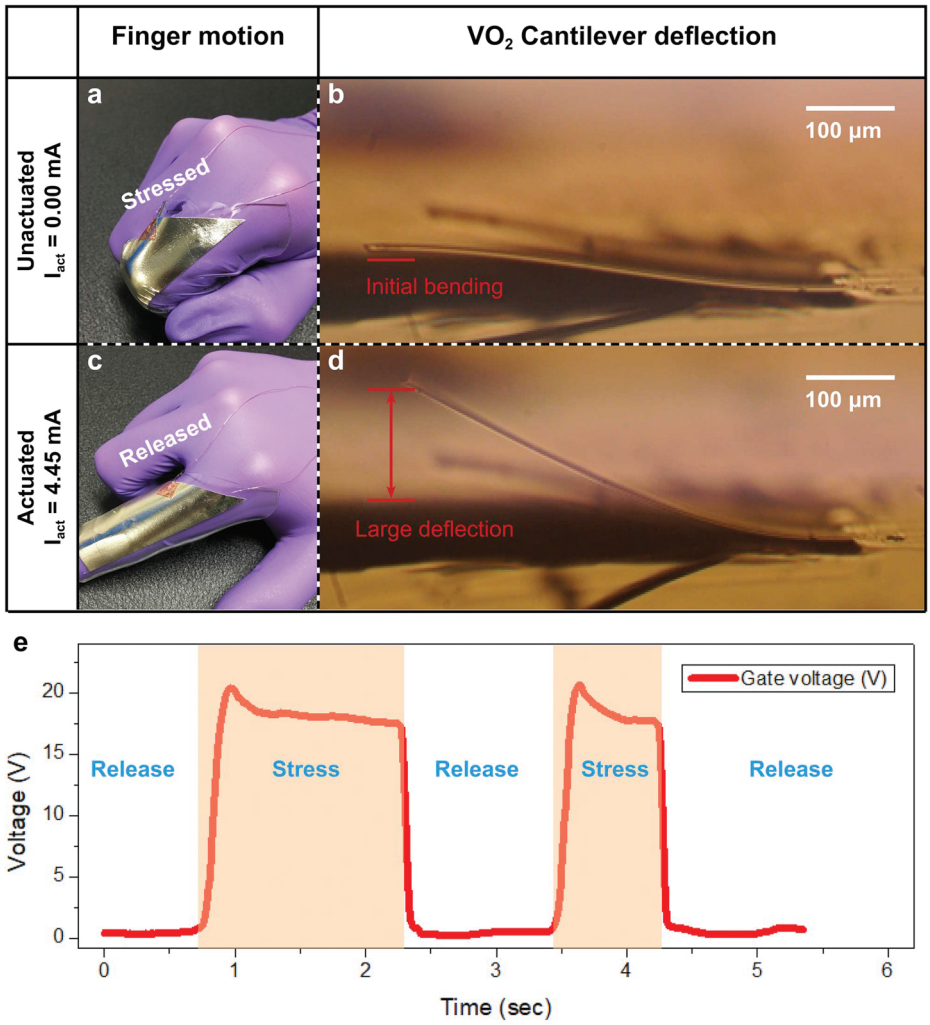

Fig. 5. FENG-based micro robotic arm controller. (a) Stress applied to the FENG device. (b) VO_2-based MEMS actuator without applying actuation current. (c) Stress released from the FENG device. (d) VO_2-based MEMS actuator with the maximum deflection at actuation current of 4.45 mA. (e) The gate voltage of the p-channel MOSFET controlled by the output of FENG, the voltage change tracks the motion of the finger.

the changing rate of the dipole moment. Hence, a second-order system is used to describe the electrical domain. The electromechanical lumped parameter model and its equivalent electrical circuit are shown in Fig. 3a and b respectively. The variable φ represents the transduction from the mechanical domain to the electrical domain.

The derived lumped model can be used to compare the outputs due to a sinusoidal input used in Fig. 2a. Fig. 3c shows the pressure due to a sinusoidal input. Fig. 3d shows the I_{sc} under this sinusoidal pressure input. The transduction to the electrical domain involves differentiating the mechanical input with respect to time. When the load (R_2) equals zero (i.e. short circuit condition), the system presents an underdamped response with the strongest oscillation as shown in Fig. 3d. Based on the derived model, it is possible to predict the electric output under different resistive loads. When the resistance of the load increases, the system evolves from an underdamped system to an overdamped system. The oscillation will decrease with increasing load resistance and the output voltage (V_{load}) changes its profile from an I_{sc}-like signal to a V_{oc}-like signal. Fig. 3e shows the measured electromechanical response under different resistive loads. The large transient oscillation only occurs with low resistive loads. It should also be noted how the measured output voltage profile keeps approaching the open circuit voltage and input pressure profiles shown in Fig. 2a. This means that the profile (and value) of the measured open circuit voltage will be highly dependent on the internal resistance of the instrument used –more details in Supporting Information. Fig. 3f shows the simulated response based on the model shown in Fig. 3b, where the parameter C_1 is 32 pF (which is the capacitance of the PPFE film), C_2 and L are chosen to be 0.15 nF and 2000 H in order to fit the experimental data. The system exhibits an underdamped response for low resistive loads and an overdamped response for higher resistance loads.

As discussed above, the V_{oc} is proportional to the input mechanical pressure amplitude and is independent of its rate of change with time. However, most of the commercial voltmeters have internal resistances in the range of 1 ~ 10 MΩ. When using such low-impedance instruments to measure V_{oc}, the measurement is misleading, since it is actually the voltage drop across a resistive load V_{load}, which can be approximated by I_{sc} times the internal resistance R_{in} of the voltmeter. Thus, V_{load} changes with both: pressure amplitude and its rate of change with time. Because the FENG is able to output a voltage signal which depends on the input pressure profile, no external power supply is required for device operation as a pressure sensor (i.e. FENG can be implemented as a self-powered flexible dynamic pressure sensor). In this work, the electromechanical response is characterized for a 15 mm × 15 mm single layer FENG device and the V_{load} is measured by using a voltmeter with 1 MΩ resistive internal resistance (NI9201, National Instruments). Given that the sinusoidal pressure input can be expressed by

$P = P_{max} sin(2\pi ft)$, where P_{max} is the peak pressure amplitude, f is the frequency; V_{load} can be expressed as:

$$V_{load} = \alpha P_{max} f cos(2\pi ft), \quad (3)$$

where $\alpha = 2\pi A P_0 R_{in}/E$. The maximum value V_{peak} is therefore found to be at $V_{peak} = V_{load}(t = 0)$ and is linearly related to $P_{max}f$. Fig. 4a and Fig. 4b show the 3D surface plot of the V_{peak} as a function of the input pressure amplitude and frequency. By fitting the data into a polynomial function, the relation between V_{peak}, P_{max}, and f can be given by: $V_{peak} = 3.1 \times 10^{-7} P^{1.1} f^{0.85}$, which is expected from Eq. (3).

A single FENG-based pressure sensor can be easily integrated into a N × N array of pressure sensor by a specific arrangement of the positive electrodes. Fig. 4c shows an array of 16 individual FENG devices, each with an area of 15 mm × 15 mm. All the elements in the array are equally spaced in both the X and Y directions. A common negative electrode is patterned on the back side of the PPFE film. To protect the silver electrodes from wearing during repeated use and humidity, the device is encapsulated into a polydimethylsiloxane (PDMS) protective layer (See detailed fabrication process in Supporting Information). Since the positive electrodes are electrically insulated from each other, each electrode can be taken as an independent pixel pressure sensor (See Movie S2, Supporting Information). Hence, this 4 × 4 matrix pressure sensor with a resolution of 16 pixels can be implemented to map the distribution of an impact. Fig. 4c shows the 3D contour map of the pressure distribution upon an external impact from the user's hand press. The different magnitudes of pressures are labeled and presented in different colors (See Fig. S7 in Supporting Information for 2D contour map of pressure distributions). The pressure distribution under different impacts is also presented (See Movie S1, Supporting Information).

Supplementary data related to this article can be found at https://doi.org/10.1016/j.nanoen.2019.06.048.

Due to FENG's large internal impedance, almost any commonly used voltmeters could cause a discharge of the self-charged electrical energy in the device and results in a transient signal output. Thus, the application is limited to dynamic pressure monitoring. When static response needs to be addressed, an electronic switch can be induced where the FENG can be used to control the gate voltage. Here we demonstrate this application by using a micro-robotic arm controlled through the movement of human body (e.g. movement of a finger) by combining the FENG and a VO_2-based bimorph microelectromechanical systems (MEMS) actuator (See Supporting Information and Movie S3). The VO_2-based actuator can be thermally actuated by utilizing the large difference in the thermal expansion coefficient of the VO_2 coating and SiO_2 substrate in the bimorph beam structure [37,38] (Fig. S11 and Fig. S12, Supporting Information). VO_2 is a first order solid-to-solid phase change smart material which undergoes a fully reversible insulator-to-metal transition (IMT). The transition typically happens at ~ 68 °C and spans ~ 15 °C [39]. During the transition, the crystal structure changes from the monoclinic phase to the tetragonal phase, leading to a ~ 1.7% shrink in the c-axis [40]. When VO_2 is deposited on top of a silicon dioxide (SiO_2) microcantilever, large compressive stress will be induced due to the crystal structural change during the phase transition. Therefore the beam structure bends up towards the out of plane direction (Fig. S12, Supporting Information). In this work, the VO_2-based MEMS actuator has dimensions of 550 μm in length, 50 μm in width and 2.3 μm in thickness. The actuation is induced by applying a current to the resistive metal heater which is embedded into the beam material. The fabrication process of the VO_2 actuator is described in detail in the Supporting Information. To enable the control of the deflection of the VO_2 actuator, a single layer FENG device of 15 mm × 35 mm is fabricated and encapsulated into a PDMS ring structure and then put onto the user's finger. As shown in Fig. 5, the FENG senses the stress coming from the flexing of the finger, and the voltage output is used to control the actuation current through the gate terminal of a p-channel metal-oxide-semiconductor field-effect transistor (MOSFET), which in turn controls the current through the VO_2-based MEMS actuator (See Supporting Information for details).

Supplementary data related to this article can be found at https://doi.org/10.1016/j.nanoen.2019.06.048.

3. Conclusion

In this work, a polypropylene ferroelectret polymer thin film with the large piezoelectric effect is presented. The discussion is mainly focused on the design platform for implementing the PPFE film as a flexible pressure sensor. Both static and dynamic pressure responses are studied when different device-machine interfaces are considered. The characterizations in terms of V_{oc} and I_{sc} are performed on a 15 mm × 15 mm single layer FENG thin patch under different mechanical impacts provided by a vibration exciter. The results show that the energy conversion process from mechanical to electrical domain could be significantly affected by the internal impedance of instruments. Measurement results can also be affected by the instrument sampling rate since the transient oscillation signal occurs at the starting edge within a short time window. A lumped parameter model is also proposed to explain the load-dependent voltage measurement variations and the results are validated by the experiment. Applications in terms of pixelated sensor array and human-robotic control interface are also demonstrated at the end. This paper provides useful information in the design of sensor/machine interface, especially when polymer-based sensor with high internal impedance is used, and in troubleshooting the variations caused by instruments.

Acknowledgement

This work was supported by the National Science Foundation (NSF ECCS Award: ECCS-1744273), and by an MSU Strategic Partnership Grant (16-SPG-Full-3236). The authors also would like to thank the Composite Materials and Structures Center (CMSC) at Michigan State University.

Appendix A. Supplementary data

Supplementary data to this article can be found online at https://doi.org/10.1016/j.nanoen.2019.06.048.

References

[1] Zhaoyao Zhan, Rongzhou Lin, Van-Thai Tran, Jianing An, Yuefan Wei, Hejun Du, Tuan Tran, Wenqiang Lu, Paper/carbon nanotube-based wearable pressure sensor for physiological signal acquisition and soft robotic skin, ACS Appl. Mater. Interfaces 9 (43) (2017) 37921–37928.
[2] Seyed Reza Larimi, Hojatollah Rezaei Nejad, Michael Oyatsi, O'Brien Allen, Mina Hoorfar, Homayoun Najjaran, Low-cost ultra-stretchable strain sensors for monitoring human motion and bio-signals, Sensor Actuator Phys. 271 (2018) 182–191.
[3] Yun Choi Dong, Min Hyeong Kim, Yong Suk Oh, Soo-Ho Jung, Jae Hee Jung, Hyung Jin Sung, Hyung Woo Lee, Hye Moon Lee, Highly stretchable, hysteresis-free ionic liquid-based strain sensor for precise human motion monitoring, ACS Appl. Mater. Interfaces 9 (2) (2017) 1770–1780.
[4] Xiaoyi Meng, Qian Cheng, Xiaobei Jiang, Zhen Fang, Xianxiang Chen, Shaoqing Li, Chenggang Li, Chunwen Sun, Wuhong Wang, Zhong Lin Wang, Triboelectric nanogenerator as a highly sensitive self-powered sensor for driver behavior monitoring, Nano Energy 51 (2018) 721–727.
[5] Weixing Song, Baoheng Gan, Tao Jiang, Yue Zhang, Aifang Yu, Hongtao Yuan, Ning Chen, Chunwen Sun, Lin Wang Zhong, Nanopillar arrayed triboelectric nanogenerator as a self-powered sensitive sensor for a sleep monitoring system, ACS Nano 10 (8) (2016) 8097–8103.
[6] Abdul Razak, Abdul Hadi, Aladin Zayegh, K Begg Rezaul, Yufridin Wahab, Foot plantar pressure measurement system: a review, Sensors 12 (7) (2012) 9884–9912.
[7] M Almassri Ahmed, WZ Wan Hasan, Ahmad Siti Anom, Asnor J. Ishak, A.M. Ghazali, D.N. Talib, Chikamune Wada, Pressure sensor: state of the art, design, and application for robotic hand, J. Sens. 2015 (2015).
[8] Tian He, Yi Shu, Xue-Feng Wang, Mohammad Ali Mohammad, Zhi Bie, Qian-Yi Xie, Li Cheng, Wen-Tian Mi, Yi Yang, Tian-Ling Ren, A graphene-based resistive pressure sensor with record-high sensitivity in a wide pressure range, Sci. Rep. 5 (2015) 8603.
[9] Xiandi Wang, Lin Dong, Hanlu Zhang, Ruomeng Yu, Caofeng Pan, Lin Wang Zhong, Recent progress in electronic skin, Adv. Sci. 2 (10) (2015) 1500169.

[10] Su-Jeong Woo, Jeong-Ho Kong, Dae-Gon Kim, Jong-Man Kim, A thin all-elastomeric capacitive pressure sensor array based on micro-contact printed elastic conductors, J. Mater. Chem. C 2 (22) (2014) 4415–4422.
[11] I Tiwana Mohsin, Stephen J. Redmond, H Lovell Nigel, A review of tactile sensing technologies with applications in biomedical engineering, Sensor Actuator Phys. 179 (2012) 17–31.
[12] Keun Young Lee, Hong-Joon Yoon, Tao Jiang, Xiaonan Wen, Wanchul Seung, Sang-Woo Kim, Lin Wang Zhong, Fully packaged self-powered triboelectric pressure sensor using hemispheres-array, Adv. Energy Mater. 6 (11) (2016) 1502566.
[13] Xiandi Wang, Hanlu Zhang, Lin Dong, Xun Han, Weiming Du, Junyi Zhai, Caofeng Pan, Lin Wang Zhong, Self-powered high-resolution and pressure-sensitive triboelectric sensor matrix for real-time tactile mapping, Adv. Mater. 28 (15) (2016) 2896–2903.
[14] Pinyo Puangmali, Kaspar Althoefer, D Seneviratne Lakmal, Declan Murphy, Prokar Dasgupta, State-of-the-art in force and tactile sensing for minimally invasive surgery, IEEE Sens. J. 8 (4) (2008) 371–381.
[15] Kwi-Il Park, Hwan Son Jung, Geon-Tae Hwang, Kyu Jeong Chang, Jungho Ryu, Min Koo, Insung Choi, Seung Hyun Lee, Myunghwan Byun, Lin Wang Zhong, Highly-efficient, flexible piezoelectric pzt thin film nanogenerator on plastic substrates, Adv. Mater. 26 (16) (2014) 2514–2520.
[16] Minjeong Ha, Jonghwa Park, Youngoh Lee, Hyunhyub Ko, Triboelectric generators and sensors for self-powered wearable electronics, ACS Nano 9 (4) (2015) 3421–3427.
[17] Lin Wang Zhong, Jinhui Song, Piezoelectric nanogenerators based on zinc oxide nanowire arrays, Science 312 (5771) (2006) 242–246.
[18] Yi-Feng Lin, Jinhui Song, Yong Ding, Shih-Yuan Lu, Lin Wang Zhong, Piezoelectric nanogenerator using cds nanowires, Appl. Phys. Lett. 92 (2) (2008) 022105.
[19] Jong Hoon Jung, Minbaek Lee, Jung-Il Hong, Yong Ding, Chih-Yen Chen, Li-Jen Chou, Zhong Lin Wang, Lead-free nanbo3 nanowires for a high output piezoelectric nanogenerator, ACS Nano 5 (12) (2011) 10041–10046.
[20] Sung-Ho Shin, Young-Hwan Kim, Min Hyung Lee, Joo-Yun Jung, Junghyo Nah, Hemispherically aggregated batio$_3$ nanoparticle composite thin film for high-performance flexible piezoelectric nanogenerator, ACS Nano 8 (3) (2014) 2766–2773.
[21] Kwi-Il Park, Minbaek Lee, Ying Liu, San Moon, Geon-Tae Hwang, Guang Zhu, Ji Eun Kim, Sang Ouk Kim, Do Kyung Kim, Zhong Lin Wang, Flexible nanocomposite generator made of batio$_3$ nanoparticles and graphitic carbons, Adv. Mater. 24 (22) (2012) 2999–3004.
[22] Yaping Zang, Fengjiao Zhang, Chong-an Di, Daoben Zhu, Advances of flexible pressure sensors toward artificial intelligence and health care applications, Mater. Horizons 2 (2) (2015) 140–156.
[23] Qingshen Jing, Sohini Kar-Narayan, Nanostructured polymer-based piezoelectric and triboelectric materials and devices for energy harvesting applications, J. Phys. D Appl. Phys. 51 (30) (2018) 303001.
[24] Youfan Hu, Zijian Zheng, Progress in textile-based triboelectric nanogenerators for smart fabrics, Nano energy 56 (2019) 16–24.
[25] Ying-Chih Lai, Jianan Deng, Ruiyuan Liu, Yung-Chi Hsiao, Steven L. Zhang, Wenbo Peng, Hsing-Mei Wu, Xingfu Wang, Zhong Lin Wang, Actively perceiving and responsive soft robots enabled by self-powered, highly extensible, and highly sensitive triboelectric proximity-and pressure-sensing skins, Adv. Mater. 30 (28) (2018) 1801114.
[26] Jae Sang Heo, Jimi Eom, Yong-Hoon Kim, Sung Kyu Park, Recent progress of textile-based wearable electronics: a comprehensive review of materials, devices, and applications, Small 14 (3) (2018) 1703034.
[27] Yunqi Cao, Wei Li, José Figueroa, Tongyu Wang, David Torres, Chuan Wang, Zhong Lin Wang, Sepúlveda Nelson, Impact-activated programming of electro-mechanical resonators through ferroelectret nanogenerator (feng) and vanadium dioxide, Nano energy 43 (2018) 278–284.
[28] Y. Cao, J. Figueroa, J. Pastrana, W. Li, Z. Chen, Z. Wang, S. Nelson, Flexible ferroelectret polymer for self-powering devices and energy storage systems, ACS Appl. Mater. Interfaces 11 (19) (2019) 17400–17409, https://doi.org/10.1021/acsami.9b02233.
[29] Wei Li, David Torres, Tongyu Wang, Chuan Wang, Sepúlveda Nelson, Flexible and biocompatible polypropylene ferroelectret nanogenerator (feng): on the path toward wearable devices powered by human motion, Nano energy 30 (2016) 649–657.
[30] Zhenhua Luo, Dibin Zhu, Junjie Shi, Steve Beeby, Chunhong Zhang, Plamen Proynov, Bernard Stark, Energy harvesting study on single and multilayer ferroelectret foams under compressive force, IEEE Trans. Dielectr. Electr. Insul. 22 (3) (2015) 1360–1368.
[31] Lin Wang Zhong, On maxwell's displacement current for energy and sensors: the origin of nanogenerators, Mater. Today 20 (2) (2017) 74–82.
[32] Xiaofeng Wang, Simiao Niu, Yajiang Yin, Fang Yi, You Zheng, Lin Wang Zhong, Triboelectric nanogenerator based on fully enclosed rolling spherical structure for harvesting low-frequency water wave energy, Adv. Energy Mater. 5 (24) (2015) 1501467.
[33] Richard H. Brown, Piezo film: form and function, Sensor Actuator Phys. 22 (1–3) (1990) 729–733.
[34] Fabio Viola, Pietro Romano, Rosario Miceli, Gianluca Acciari, Ciro Spataro, Piezoelectric model of rainfall energy harvester, 2014 Ninth International Conference on Ecological Vehicles and Renewable Energies (EVER), IEEE, 2014, pp. 1–7.
[35] Yaowen Yang, Hao Wu, Chee Kiong Soh, Experiment and modeling of a two-dimensional piezoelectric energy harvester, Smart Mater. Struct. 24 (12) (2015) 125011.
[36] Y.C. Shu, I.C. Lien, Analysis of power output for piezoelectric energy harvesting systems, Smart Mater. Struct. 15 (6) (2006) 1499.
[37] Rafmag Cabrera, Emmanuelle Merced, Sepúlveda Nelson, Performance of electrothermally driven vo$_2$-based mems actuators, J. Microelectromech. Sys. 23 (1) (2014) 243–251.
[38] Yunqi Cao, David Torres, Tongyu Wang, Xiaobo Tan, Sepúlveda Nelson, Enabling tunable micromechanical bandpass filters through phase-change materials, Smart Mater. Struct. 26 (8) (2017) 085032.
[39] F.J. Morin, Oxides which show a metal-to-insulator transition at the neel temperature, Phys. Rev. Lett. 3 (1) (1959) 34.
[40] T.J. Huffman, C. Hendriks, E.J. Walter, Joonseok Yoon, Honglyoul Ju, R. Smith, G.L. Carr, H. Krakauer, M.M. Qazilbash, Insulating phases of vanadium dioxide are mott-hubbard insulators, Phys. Rev. B 95 (7) (2017) 075125.